Quantitative Hybridization Kinetics of DNA Probes to RNA in Solution Followed by Diffusional Fluorescence Correlation Analysis†

Petra Schwille,* Frank Oehlenschläger,‡ and Nils G. Walter§

Max-Planck-Institute for Biophysical Chemistry, Department of Biochemical Kinetics, Am Fassberg, D-37077 Göttingen, Germany

Received March 1, 1996; Revised Manuscript Received May 31, 1996⊗

ABSTRACT: Binding kinetics in solution of six *N*,*N*,*N*′,*N*′-tetramethyl-5-carboxyrhodamine-labeled oligodeoxyribonucleotide probes to a 101mer target RNA comprising the primer binding site for HIV-1 reverse transcriptase were characterized using fluorescence correlation spectroscopy (FCS). FCS allows a sensitive, non-radioactive real time observation of hybridization of probes to the RNA target in the buffer of choice without separation of free and bound probe. The binding process could directly be monitored by the change in translational diffusion time of the 17mer to 37mer DNA probe upon specific hybridization with the larger RNA target. The characteristic diffusion time through a laser-illuminated open volume element with 0.5 μm in diameter increased from 0.13−0.2 ms (free) to 0.37−0.50 ms (bound), depending on the probe. Hybridization was approximated by biphasic irreversible second-order reaction kinetics, yielding first-phase association rate constants between 3×10^4 and 1.5×10^6 M^{-1} s^{-1} for the different probes. These varying initial rates reflected the secondary structures of probes and target sites, being consistent with a hypothetical binding pathway starting from loop−loop interactions in a kissing complex, and completion of hybridization requiring an additional interaction involving single-stranded regions of both probe and target. FCS thus permits rapid screening for suitable antisense nucleic acids directed against an important target like HIV-1 RNA with low consumption of probes and target.

Hybridization of nucleic acids to their complementary sequences is a fundamental process in molecular biology. It plays a major role in replication, transcription, and translation, where specific recognition of nucleic acid sequences by complementary strands is essential for propagation of information content. In most of these processes, RNA participates as the naturally occurring single-stranded nucleic acid form, ready to hybridize. Competing with hybridization to another single-stranded molecule, formation of secondary structure via intramolecular hydrogen bonds can occur. The secondary structure of RNA is also involved in other processes like binding of specific proteins, hydrolysis within the cellular environment, or transcription and translation control (Ma et al., 1994; Yang et al., 1995; Varani, 1995).

In the case of naturally occurring antisense RNAs, hybridization plays a negative feedback role. These molecules specifically bind to their complementary sequences and thereby block functionality of sense RNA (Simons, 1988; Wagner & Simons, 1994). This has been used to design artificial antisense RNAs to down-regulate target gene expression (Inouye, 1988; van der Krol et al., 1988; Wagner, 1994). Both RNA and DNA probes are currently employed to suppress viral replication, a method that might become a therapeutic tool to particularly fight pathogenic retroviruses (Crooke, 1992; Dropulic & Jeang, 1994). With viruses such as HIV-1, the viral RNA is simultaneously a target for hybridization of the replication primer (typically a host tRNA) and the therapeutic antisense nucleic acid, both being in competition with secondary structure formation of their target sites (Lima et al., 1992; Isel et al., 1995). Consequently, hybridization between complementary strands is complex and initiates at loops or bulges within the secondary structure, followed by rapid zippering leading to fully double-stranded hybrid (Wagner & Simons, 1994; Hjalt & Wagner, 1995). It is therefore not surprising that the performance of a particular antisense nucleic acid is often not predictable within a host cell, where both target and antisense strand might be inaccessible due to higher order structures and complexation with proteins or hybridization might simply be unfavorable because of ionic conditions and low concentrations.

A better understanding of RNA hybridization to complementary strands in solution could provide deeper insights into the described fundamental biological and technological processes. Thus, it becomes necessary to perform kinetic analyses of nucleic acid hybridization. Classically, these analyses have been performed to understand gene structure and function, especially genome complexity and gene copy number (Britten & Kohne, 1968; Young & Anderson, 1985). The basic requirement for a quantitative study on nucleic acid hybridization in solution is to separately monitor paired and unpaired strands. In the past, this has been achieved using physical methods like absorbance spectroscopy (hypochromicity or circular dichroism; Bush, 1974), calorimetry (Breslauer, 1986), or nuclear magnetic resonance (Patel et al., 1982). Generally, these techniques require quite considerable amounts of nucleic acids in the microgram to milligram range. Radioactive labeling allows detection of

† This work was supported by Grant No. 0310739 from the German Ministry for Education, Science, Research, and Technology. Financial support by EVOTEC BioSystems GmbH, Hamburg, to P.S. and F.O. is gratefully acknowledged.

* Author to whom correspondence should be addressed. Tel: +49-551-201-1436. FAX: +49-551-201-1435.

‡ This author should be regarded as also having first author status.

§ Present address: University of Vermont, Department of Microbiology and Molecular Genetics, Burlington, VT 05405.

⊗ Abstract published in *Advance ACS Abstracts,* July 15, 1996.

S0006-2960(96)00517-X CCC: $12.00

minute amounts of nucleic acids and has been used for direct analysis of solution hybridization on non-denaturing gels (Kumazawa et al., 1992) or by chromatographic methods (Dewanjee et al., 1994) and for enzymatic assays like resistance to nuclease S1 (Bishop et al., 1974) or RNase H (Zarrinkar & Williamson, 1994). With these isotopic assays, physical separation of hybridized and unhybridized strands is required, e.g., by precipitation, solid phase capturing, electrophoresis, or chromatography. This makes true solution-phase measurements impossible.

Recently, sensitive fluorescence measurements have been used to directly monitor nucleic acid hybridization in solution. One approach uses a fluorophore on the 5′ end of one strand and a quenching dye on the 3′ end of the complementary strand. Hybridization is then monitored by decreasing fluorescence of the donor and increasing fluorescence of the acceptor due to starting energy transfer (Morrison & Stols, 1993). This technique requires two fluorescent labels at different sites and so far has been limited to hybridization studies of complementary DNAs forming a blunt-ended hybrid. In an analogous approach, the same strand is labeled with a donor on the 3′ end and an acceptor on the 5′ end and energy transfer decreases after hybridization (Parkhurst & Parkhurst, 1995). With certain fluorophores like pyrene, the detection of hybridization to a complementary strand is possible due to altered quenching effects of base-paired nucleobases on the dye. Either DNA−DNA (Manoharan et al., 1995) or RNA−RNA hybridization in solution (Li et al., 1995) can thus be monitored, but typically quite high (micromolar) concentrations of the labeled strand are required.

Fluorescence correlation spectroscopy (FCS)[1] is a technique developed to study dynamic processes of fluorescent molecules that give rise to fluorescence fluctuations (Magde et al., 1972, 1974; Elson & Magde, 1974; Ehrenberg & Rigler, 1974; Koppel, 1974). Since its introduction, the technique has found a broad range of applications, like measurement of diffusion constants, chemical kinetic rate constants, and molecular weights [for review, see Thompson (1991)]. Recently improved setups use an epi-illuminated microscope with strong focusing of the exciting laser beam and a small pinhole with an avalanche diode for detection, e.g., to analyze translational diffusion in dilute solutions (Rigler et al., 1992, 1993). Kinjo and Rigler (1994) were thus able to follow the binding of a fluorescently labeled 18mer DNA primer at a concentration of 50 nM to a 7.5 kb DNA containing the complementary sequence by monitoring the slowing down of primer diffusion through the laser beam.

To understand hybridization to RNA strands, we have been interested in hybridization kinetics of DNA probes to RNAs. Here, FCS seemed to be an appropriate tool, since it allows direct observation of hybridization without physical separation of strands, but with high sensitivity and requiring only the DNA strand to be labeled with a single, freely eligible fluorophore. Since many biologically relevant RNAs (like tRNAs or ribozymes) are often between 70 and 700 bases in length and since diffusion times (being inversely related to diffusion coefficients) are in first approximation proportional to the third root of the molecular weight of the diffusing species (according to the Stokes−Einstein relation), the increase in diffusion time of the labeled probe upon hybridization can be expected to be low and quantitative values of hybridized fractions difficult to extract. In the present work, we therefore used an artificial short-chained RNA comprising the replicative primer binding site of HIV-1 to rigorously prove that FCS can measure quantitative kinetic constants for this kind of hybridization targets. The 101mer RNA folds into a secondary structure with two stem−loop domains (Figure 1) and has been used in our laboratory as template for *in vitro* replication studies with reverse transcriptases (Pop, 1995; Gebinoga & Oehlenschläger, 1996). We designed six *N*,*N*,*N*′,*N*′-tetramethyl-5-carboxyrhodamine (TMR)-labeled DNA probes with equal calculated melting points against different regions of the target (Figure 1) and were able to directly monitor the increase in their diffusion times upon binding in solution by a shift in the autocorrelated fluorescence signal. Using appropriate controls, quantitative data for the ratio of bound to unbound species at a total concentration of 10 nM could be extracted and compared to values obtained by a non-radioactive primer extension assay using the same fluorescent probes. Thus, it could be shown that DNA−RNA hybridization kinetics as a function of target and probe secondary structure can directly and sensitively be followed using FCS.

MATERIALS AND METHODS

Materials. Target α-1 RNA is a 101-nucleotide *in vitro* transcript of the plasmid HP18α-1, linearized with *Hin*dIII (Pop, 1995), its concentration being determined by the assumption that 1 OD_{260} equals 40 μg/mL. It shows a secondary structure with some double-stranded regions (Figure 1). Using the Vienna RNA package computer program (Hofacker et al., 1994), a denaturation temperature of about 70 °C was calculated. The six DNA probes HS1 to HS6 are labeled with the 5-isomer of TMR at their 5′ end via an aminohexyllinker (Figure 2) and were purchased in HPLC-pure quality from NAPS (Göttingen, Germany). Their purity was again controlled by HPLC (monitoring absorbances at 260 and 554 nm), their concentration determined taking into account, that the TMR label contributes to the absorbance at 260 nm (with $A_{260}/A_{554} = 0.49$) and the degree of substitution (DOS) confirmed to be one label per molecule using the equation $DOS = [(10N/86)A_{554})]/[A_{260} - (0.49 \times A_{554})]$ (with N the number of bases in the probe). Sequences were as follows: 19mer HS1, 5′-TMR-d(GACATTGTTCGTCGGCCGC); 29mer HS2, 5′-TMR-d(CATCAATGTCAATAAGGTGACATTGTTCG); 37mer HS3, 5′-TMR-d(TGCTAGAGATCTCTAAGTTATAACACATCAATGTCAA); 30mer HS4, 5′-TMR-d(GGCGCCACTGCTAGAGATCTCTAAGTTATA); 17mer HS5, 5′-TMR-d(GTCCCTGTTCGGGCGCC); 23mer HS6, 5′-TMR-d(AGCTTCCCTTTCGCTTTCA GGTC). The probes were chosen such that each probe's complex with its cDNA would melt in hybridization buffer at about 77 °C, suggesting uniform thermodynamic parameters for the RNA−DNA hybrids as well. HS1X−HS6X are the corresponding unlabeled probes and GSHS1−GSHS6 are the length-matched cDNA strands of HS1−HS6, respectively, all being synthesized on a Milligene Expedite Synthesizer. HIV-1

[1] Abbreviations: FCS, fluorescence correlation spectroscopy; kb, kilo bases; TMR, *N*,*N*,*N*′,*N*′-tetramethyl-5-carboxyrhodamine; HIV, human immunodefficiency virus; HPLC, high-performance liquid chromatography; DOS, degree of substitution; bp, base pairs; PAGE, polyacrylamide gel electrophoresis; PACE, polyacrylamide capillary electrophoresis.

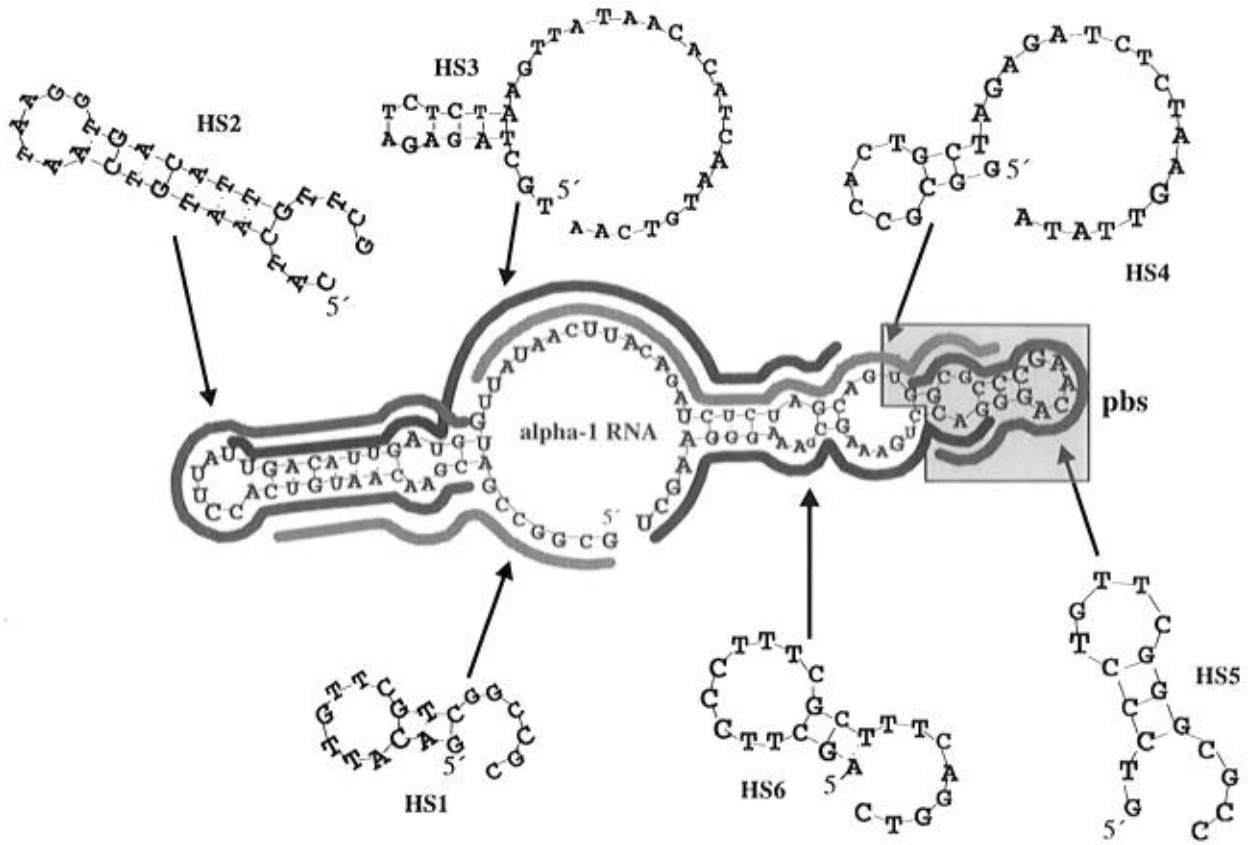

FIGURE 1: Secondary structure models for the six DNA probes HS1 to HS6 and target α-1 RNA. The 5′ TMR-labeled probes are designed to hybridize with different target sites, represented by shaded lines. The primer binding site (pbs) of HIV-1 reverse transcriptase is highlighted by a shaded bar.

reverse transcriptase was a grateful donation from Dr. Magda Pop and purified from an overexpressing *Escherichia coli* strain as described (Müller et al., 1989). Sonicated salmon sperm DNA was from Stratagene (Heidelberg, Germany). dNTPs were obtained from Pharmacia (Freiburg, Germany), while TMR-labeled UTP was custom-made by NAPS (Göttingen, Germany).

Hybridization Protocols. For kinetic analysis, α-1 RNA was dissolved in water to 1 μM, heated at 75 °C for 2 min to ensure complete denaturation, and allowed to cool to room temperature for 15 min. This stock solution was used to set up solution A with typically 100 nM α-1 RNA in 60 mM Tris-HCl, pH 8.2, 10 mM $MgCl_2$, 10 mM KCl, 2.5 mM DTT, 2 mM spermidine, and 10 μg of sonicated salmon sperm DNA/mL. Solution B typically contained 20 nM HS1−HS6 (60 nM in the case of HS3) in the same buffer excluding RNA. Both solutions were equilibrated separately at 40 °C for 30 min. Hybridization was initiated by mixing equal volumes of solutions A and B (typically each 50 μL) at 40 °C. 30 μL aliquots were continuously analyzed in an open sample carrier at 40 °C by FCS, being exchanged after 5 min to limit deviations due to sample evaporation, adsorption, or bleaching.

To measure a maximum value for hybridization extent, solutions A and B described above were mixed and then heated at 75 °C for 2 min. The mixture was cooled to room temperature over 15 min and then incubated at 40 °C for 15 min before FCS analysis. To study dissociation, an excess of 1 μM unlabeled probe was added to the obtained hybrid and the diffusion time of the TMR-labeled probe was monitored over 2 h.

For hybridization of corresponding cDNA strands with HS1−HS6, solution A contained 1 μM GSHS1−GSHS6 instead of 100 nM α-1 target RNA, and both solutions A and B were first mixed, then denatured, and cooled down as described above.

To hybridize TMR-labeled α-1 RNA with excess unlabeled probe, solution A described above contained 20 nM TMR-labeled α-1 RNA, while solution B included 1 μM unlabeled HS1X−HS6X. Both solutions were again mixed prior to denaturation and cooled down as described above.

To measure the diffusion time of α-1 RNA in dependence of initial RNA concentration, 125 nM TMR-labeled α-1 RNA was mixed with 1.25 μM unlabeled α-1 RNA and diluted to give total RNA concentrations of 1.38 μM, 550 nM, 275 nM, and 138 nM in water. An additional solution contained 40 nM TMR-labeled α-1 RNA. These solutions were heated at 75 °C for 2 min, cooled to room temperature over 15 min, diluted to a final concentration of 138 nM RNA (40 nM for the fifth solution) in hybridization buffer (60 mM Tris-HCl, pH 8.2, 10 mM $MgCl_2$, 10 mM KCl, 2.5 mM DTT, 2 mM spermidine, and 10 μg of sonicated salmon sperm DNA/mL), and analyzed by FCS.

FCS Measurement and Extraction of Diffusion Times and Hybrid Fractions. Fluorescence correlation spectroscopy is a special case of fluctuation correlation spectroscopy, where temporal fluctuations in a sample of laser-excited fluorescent molecules are self-correlated to obtain information about the processes leading to fluorescence fluctuations. These underlying processes may be photophysical transitions, shifts in wavelength, changes in quantum yield, or simply concentration fluctuations by thermal motion (diffusion) of the

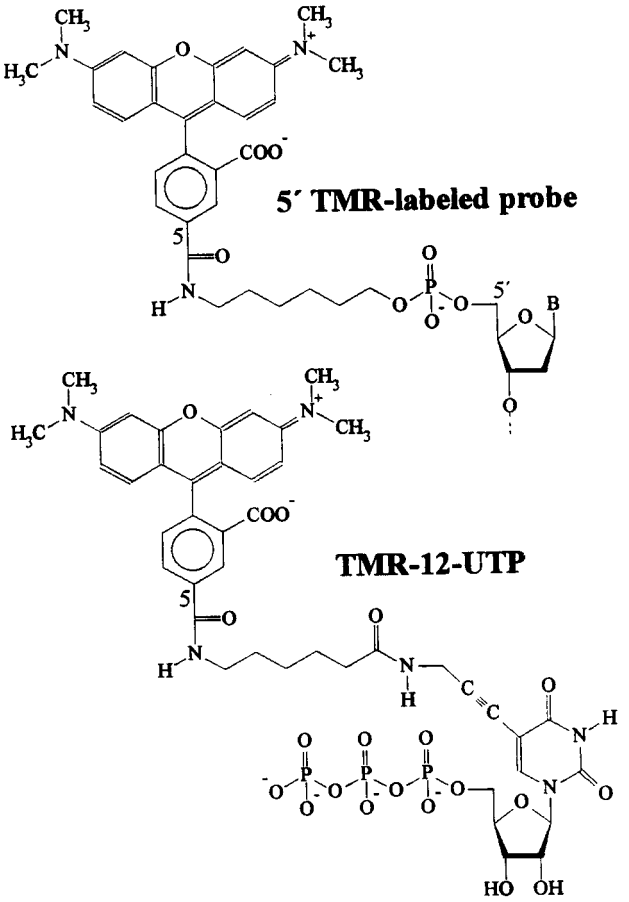

FIGURE 2: Molecular structures of the N,N,N′,N′-tetramethyl-5-carboxyrhodamine (TMR) labels used in this study for fluorescent detection. DNA probes were 5′ end-labeled with TMR-succinimidyl ester via an aminohexyl linker, while RNA was internally labeled by transcription in the presence of TMR-12-UTP.

fluorophores. In solutions with diffusing species, both the magnitude $G(0)$ and the rate and shape of the temporal decay of the autocorrelation function $G(t)$ have previously been used to detect concentrations and characterize molecular aggregation (Palmer & Thompson, 1989; Thompson, 1991). The temporal decay of $G(t)$ allows extraction of the characteristic time for diffusion of the fluorophores, which may change upon interaction with non-fluorescent molecules. This latter principle was used earlier to analyze binding of fluorescently labeled antigens or antibodies to latex particles (Briggs et al., 1981) or of DNA probes to a DNA target (Kinjo & Rigler, 1994) and was exploited in the present study for analysis of DNA−RNA hybridization.

Figure 3 describes our experimental setup. The 514 nm line of an argon ion laser (Lexel 85, power 0.2 mW) epi-illuminates a Zeiss water immersion 63 × 1.2 microscope objective without any prefocusing system. The sample droplet (30 μL) is placed into a gold-covered, chemically inert open sample carrier (Walter & Strunk, 1994) thermostated at 40 °C, and the objective surface is directly lowered onto the solution. Evaporation is minimized by close contact between sample carrier and objective, and adsorption and bleaching effects are reduced by exchange of the sample droplet after 5 min against solution separately incubated at 40 °C in a closed, light-shielded tube. The wavelength-shifted fluorescence light in opposite direction now traverses the dichroic mirror, passing a 565 DF 50 bandpass filter (Omega Optics) to suppress background light such as Raman scattering or laser reflections. The 50 μm diameter pinhole in the image plane defines the z-dimension of the analyzed sample volume and is imaged 1:1 onto the detector surface of an avalache photodiode (EG&G SPCM-200). The photocount signal was autocorrelated over 1 min (30 s for the first measurement after hybridization start) quasi-online by a digital signal correlator card (ALV-5000, Fa. Peters, Langen, Germany).

The autocorrelation function $G_1(t)$ for fluctuations in a diffusional system with a single sort of fluorescent particles depends on the average number of fluorophores N in the illuminated volume element of the sample (i.e., their concentration), the average translational diffusion time τ_{diff} (given by the xy-radius r of the volume element and the diffusion coefficient D to $\tau_{diff} = r^2/4D$), and the structure parameter of the volume element r/z (radius divided by half of the length), which is constant for a defined setup, in our case 0.2. Using the pinhole as optical field diaphragm (Qian & Elson, 1991), the three-dimensional shape of the illuminated detection volume element can be approximated as Gaussian in all directions (Rigler et al., 1993). This defines $G_1(t)$ to be (Thompson, 1991; Rigler et al., 1993):

$$G_1(t) = \frac{1}{N}\frac{1}{1+\frac{t}{\tau_{diff}}}\frac{1}{\sqrt{1+\left(\frac{r}{z}\right)^2\frac{t}{\tau_{diff}}}} \quad (1)$$

In the case of singlet−triplet transitions of the fluorophores and with T being the average fraction of dye molecules in triplet state with a relaxation time τ_{tr}, this changes to (Widengren et al., 1994, 1995):

$$G_{1,T}(t) = (1 - T + Te^{-t/\tau_{tr}})G_1(t) \quad (2)$$

The principle of hybridization detection is based on the sensitivity of FCS to changes in the average translational diffusion time. For a system of M diffusing species labeled with fluorophores of comparable triplet decay times, and with Y_i being their fractions ($\sum Y_i = 1$), the general autocorrelation function is given by:

$$G_{M,T}(t) = \frac{(1 - T + Te^{-t/\tau_{tr}})}{N}\sum_{i=1}^{M}\frac{Y_i}{1+t/\tau_i}\frac{1}{\sqrt{1+(r/z)^2\,t/\tau_i}} \quad (3)$$

If the diffusion times τ_i of the different components are known, the fractions can be determined in a sample droplet by mathematical rather than physical separation. Upon hybridization of a labeled DNA probe to its RNA target, a more slowly diffusing complex forms. The three to four times larger hybrid needs approximately twice as long to traverse the laser-illuminated volume element and remains stable throughout this diffusion time (in the range of ms), since dissociation is orders of magnitude slower. Theoretically, an $M = 2$ system is obtained, and the fraction of bound probe Y_2 increases over hybridization time. Eventual changes in triplet decay times τ_{tr} generally do not interfere with measured diffusion times, since for rhodamine dyes in water τ_{tr} are typically 2 orders of magnitude smaller and can easily be separated (Widengren et al., 1994, 1995). The dependence of triplet fraction and fluorescence quenching on

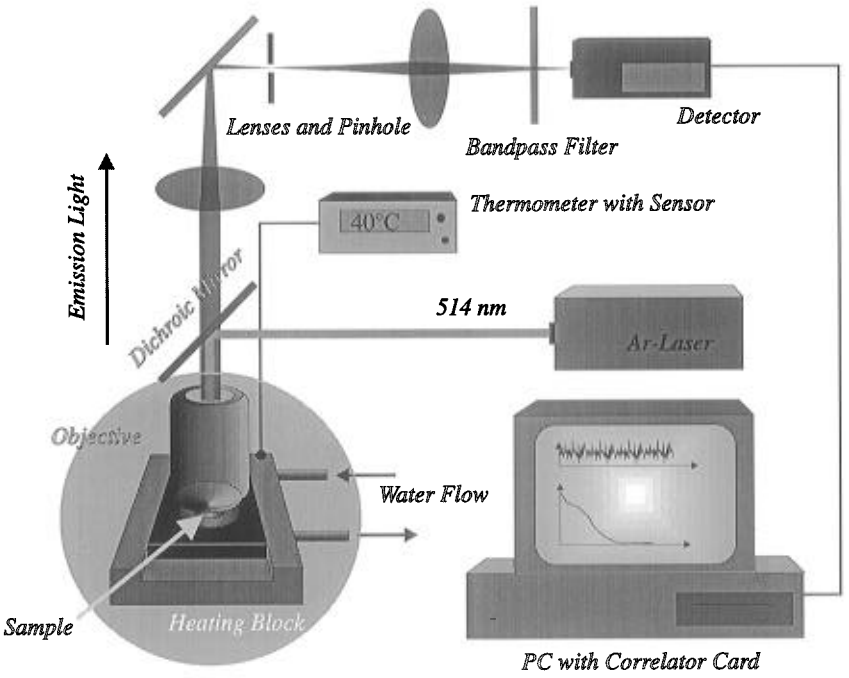

FIGURE 3: Schematic diagram of the fluorescence correlation spectroscopy (FCS) setup used in this study.

binding to target RNA was found to be negligible, as well as volume element instabilities due to temperature effects on the detection optics.

In practice, we had to include an additional diffusion time in the range of 0.01−0.04 ms to fit the autocorrelation curves of the labeled probes in the fast time range with satisfactory standard deviation. The fraction of this component was rather independent of laser intensity and slightly increased over incubation time at 40 °C. Therefore, it most likely represents either a very fast diffusing species like free fluorophore (which we did not detect by other means such as HPLC) or a bleaching term of a specific physical transition of TMR coupled to an oligonucleotide. Free probes and hybrid mixtures were evaluated by nonlinear least-squares fitting (Marquardt) of the obtained autocorrelation curves with eq 3 for $M = 2$ and $M = 3$, respectively. The diffusion time of the unknown fast component was calibrated to 0.04 ms and held constant in the fits for all probes. Since this component was independent of RNA addition, its introduction allowed better fitting of the fast time range without affecting the calculated fractions of bound probe. To reduce the number of free fitting parameters and to clearly separate τ_i for free probe and hybrid, both were first determined independently by fitting the diffusion time of the probe without RNA and of the TMR-labeled RNA with excess unlabeled probe, respectively.

In Vitro Labeling of α-1 RNA. For fluorescent labeling of α-1 RNA, an *in vitro* transcription protocol (Milligan et al., 1987) was modified to include the TMR-labeled UTP of Figure 2 (TMR-12-UTP). The labeling reaction was carried out in a total volume of 500 μL for 1 h at 37 °C with 40 mM Tris-HCl, pH 8.0, 8 mM $MgCl_2$, 50 mM NaCl, 2 mM spermidine, 5 mM DTT, 1 mM each ATP, GTP, and CTP, 0.25 mM UTP, 0.125 mM TMR-12-UTP, 2 μg of *Hin*dIII-digested plasmid HP18α-1, and 10 units of T7 RNA polymerase/mL. The TMR-labeled transcript was purified by denaturing 7% PAGE and diffusion eluted, and its absorbances at 260 and 554 nm were determined. The DOS was calculated as described above to be 27%, indicating that a major fraction of fluorescent molecules carries a single TMR label while minor fractions carry two or more fluorophores.

Quantitated Primer Extension Assay. A 20 μL aliquot of a hybridization mixture was taken, supplemented with 3.5 μL of an assay mixture to give final concentrations of 1 mM of each dNTP and 0.53 units of (360 nM) of HIV-1 reverse transcriptase/mL and incubated at 40 °C for 2 min. Primer extension was stopped by adding 390 μL of a stop-mix containing 80 μL of water, 10 μL of 3 M NaOAc, pH 5.2, and 300 μL of EtOH. The labeled probe was precipitated by centrifugation, washed once with 70% EtOH, and dried, and half of it was loaded onto an 8% sequencing gel to be analyzed by electrophoresis on a model 373A DNA sequencer as described by the manufacturer (Applied Biosystems, Weiterstadt, Germany). After completion of the gel run, intensities of the fluorescent bands showing up in the yellow "T signal" were quantified, their relative distributions calculated, and their fragment lengths determined using the Genescan 672 equipment (Applied Biosystems, Weiterstadt, Germany).

DNA Melting Curves. Automated melting curves were recorded by monitoring A_{260} as described previously (Pörschke & Jung, 1982) using a Cary 219 spectrophotometer (Varian) on solutions containing the complementary DNA oligomers both at 5 μM in the same buffer as used in the hybridization protocols (60 mM Tris-HCl, pH 8.2, 10 mM $MgCl_2$, 10 mM KCl, 2.5 mM DTT, 2 mM spermidine). Temperature was increased from 10 to 90 °C, with a heating rate of 0.1 °C/min. Melting temperatures of the hybrids were determined by nonlinear least-squares fitting of the melting curves as described (Pörschke & Jung, 1982).

RESULTS

Following Hybridization with FCS. In our setup, the principle of fluorescence correlation analysis is combined with a confocal microscope (Figure 3). This allows to

autocorrelate temporal fluctuations in a very small volume element, restricted by the focal point of an epi-illuminated objective to about 0.2 fL. The beam waist of 0.5 μm is determined by the objective characteristics like numerical aperture and magnification, the five times larger *z*-dimension of the analyzed volume element is limited by a pinhole imaged in the focal plane. Both values proved to be constant during observation time in a previous measurement of calibrated pure dye solution of known concentration and diffusion properties. Temporal autocorrelation of the fluorescence signal from this illuminated open volume element yields information about characteristic diffusion times of the fluorophores. Since association of molecules results in higher molecular weights and increased diffusion times, hybridization can be followed online by a temporal decay shift of the FCS autocorrelation curve without separation of free and bound probe.

Hybridization of the six TMR-labeled probes HS1−HS6 to their target α-1 RNA (Figure 1) was typically performed at concentrations of 10 nM probe and 50 nM RNA to obtain kinetics with characteristic times in the 10 min range that could be followed over 1 h without special equipment for very fast reactions. Lower RNA concentrations resulted in kinetics too slow to be conveniently analyzed without the risk of RNA degradation. Since α-1 RNA contains part of the HIV-1 genome and has been used as target for *in vitro* reverse transcription using the viral polymerase (Pop, 1995; Gebinoga & Oehlenschläger, 1996), an HIV-1 reverse transcription buffer with 60 mM Tris-HCl, pH 8.2, 10 mM $MgCl_2$, 10 mM KCl, 2.5 mM DTT, and 2 mM spermidine at 40 °C was used as a typical environment for the underlying DNA−RNA hybridization reactions. Sonicated salmon sperm DNA at 10 μg/mL had to be added in order to suppress unspecific adsorption of probe and target nucleic acids at low concentrations to surfaces of the reaction chamber or microscope objective. Both FCS and primer extension analysis proved that salmon sperm DNA neither associated with probes nor with TMR-labeled target RNA. Under these conditions, FCS yielded autocorrelated fluorescence signals of the probes specifically shifting over time upon addition of complementary target α-1 RNA (Figure 4). No such shift was observed without α-1 RNA or after addition of nontarget strands like MDV-1 RNA (Mills et al., 1980).

To clearly separate diffusion times of free probe and hybrid, which only differ by a factor of 2−3, and to fix them in least-squares fits of the autocorrelation curves for better analysis, both were determined in independent measurements. For this purpose, labeled probe prior to addition of target RNA, and TMR-labeled α-1 RNA (generated by *in vitro* transcription in the presence of TMR-12-UTP, Figure 2) hybridized to a 50 times excess of unlabeled probe were analyzed, respectively. Diffusion times were calculated using eq 3 and are given in Table 1. The differences in diffusion times for the six hybrids might reflect the various extents of target secondary structure perturbation (Figure 1).

Fixing the obtained diffusion times of probe and hybrid in eq 3 enabled us to easily extract the distribution of the two fluorescent diffusing species from autocorrelation curves of the hybridization mixtures. However, especially for the first reaction phase (up to 40 min) the extracted diffusion times from fitting without fixing showed to be consistent with the calibration values (average errors of 3%−7%). Integration errors caused by a 30 s data collection time in the first reaction phase can be estimated to be below 5%. Figure 5 shows the increase in hybrid fraction over time for five of the probes. The observed kinetics are quite different, with HS1, HS5, and HS6 hybridizing rapidly and HS3 and HS4 being comparably slow. HS2 showed an increase in hybrid fraction over 1 h too low to be reproducibly quantified. It is obvious that, though a 5 times (in the case of 30 nM HS3, 1.7times) excess of target over probe was used, none of the probes quantitatively forms hybrids within the observation time. Generally, after a fast initial phase, the kinetics slow down such that after 1 h a considerable portion (typically between 10% and 40%, in the case of HS2 even up to 90%) of probe remains unhybridized. A limited hybridization extent was also observed for a different hybridization protocol, where probe and target RNA were denatured together and subsequently cooled down to rapidly obtain a maximum yield of hybrid (Table 2). In order to prove that this observation was not simply due to a lack of FCS to distinguish between free and bound probe or due to a detection bias for the faster diffusing free species, a quantifiable primer extension assay was designed as an independent measure for hybridization extent.

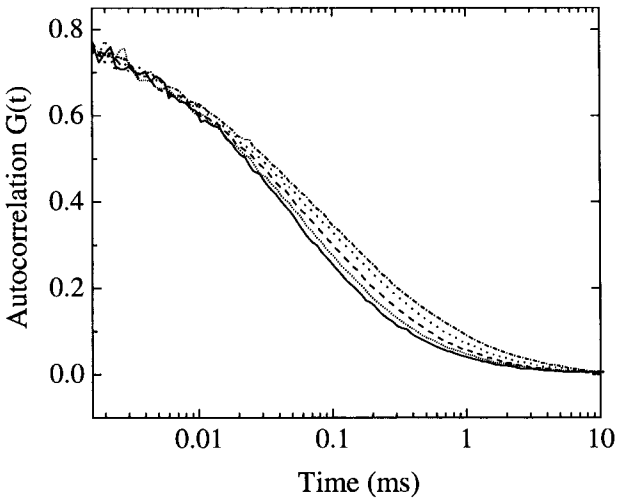

FIGURE 4: Shift over time of temporal autocorrelation $G(t)$ for 10 nM fluorescently labeled HS1 incubated with 50 nM α-1 RNA at 40 °C in hybridization buffer with 60 mM Tris-HCl, pH 8.2, 10 mM $MgCl_2$, 10 mM KCl, 2.5 mM DTT, 2 mM spermidine, and 10 μg of sonicated salmon sperm carrier DNA/mL. The half-value of the amplitude represents the average diffusion time. (Solid line, pure probe; short-dotted line, with RNA after 30 s; dashed line, after 5 min, dotted line, after 30 min; dash-dotted line, after 60 min)

Table 1: Diffusion Times of HS1−HS6, Free and Bound to α-1 RNA, through the Laser-Illuminated Open Volume Element of the FCS Setup in Hybridization Buffer at 40 °C (ms)

probe	HS1	HS2	HS3	HS4	HS5	HS6
free probe	0.15	0.18	0.21	0.20	0.11	0.15
bound probe	0.45	0.37	0.45	0.45	0.48	0.45

Comparison with Quantitated Primer Extension Assays. Since hybridization was performed in a reaction buffer for HIV-1 reverse transcriptase, the extent of hybridized TMR-labeled probe could easily be accessed by addition of this enzyme together with dNTPs at concentrations of 360 nM and 1 mM, respectively. The polymerase binds to DNA−RNA heteroduplexes with a binding constant of 5 nM (Kati et al., 1992), suggesting that the expected ⩽10 nM hybrid in the hybridization assay should be readily bound by the

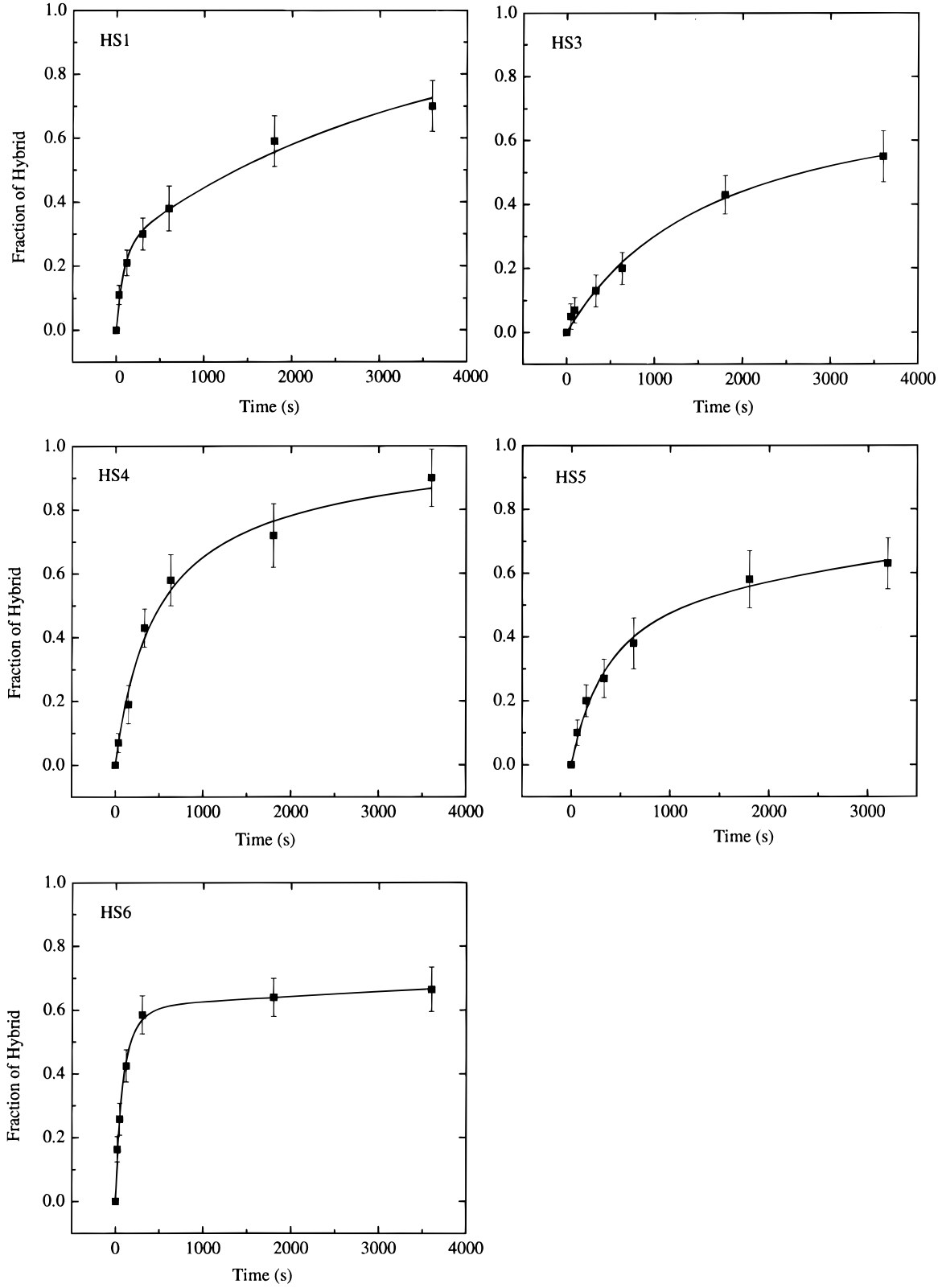

FIGURE 5: Hybridization kinetics of the probes HS1 and HS3−HS6 at 10 nM (30 nM in the case of HS3) with 50 nM α-1 RNA as measured by the shift in their autocorrelation function upon hybridization. Incubation buffer was 60 mM Tris-HCl, pH 8.2, 10 mM $MgCl_2$, 10mM KCl, 2.5 mM DTT, 2 mM spermidine, and 10 μg of sonicated salmon sperm carrier DNA/mL. Quantitative values for the bound probe fractions were calculated using eq 3 after determining the diffusion times for free probe and hybrid independently by analyzing the autocorrelation functions of probe without RNA and of TMR-labeled target with excess unlabeled probe. The solid line curves are fits obtained using eq 5.

enzyme. Moreover, HIV-1 reverse transcriptase incorporates nucleotides at a rate of 74 s^{-1} and dissociates from the DNA−RNA heteroduplex at 0.06 s^{-1} (Kati et al., 1992). Incubation for 2 min at a reaction temperature of 40 °C should therefore result in full extension of all probes hybridized to the 101mer RNA target, while free probe molecules should be unaffected. The obtained concentration of extension products was high enough to be analyzed and

Table 2: Hybridization Extent (with Standard Deviation of at Least Two Independent Measurements) after Incubation of Probe HS1−HS6 with α-1 RNA Target at 40 °C for 1 h and after Denaturation of Probe and Target Together[a]

probe	HS1	HS2	HS3	HS4	HS5	HS6
1 h at 40 °C/FCS	70 ± 6	*b*	55 ± 5	90 ± 9	60 ± 5	65 ± 5
1 h at 40 °C/E	*c*	11 ± 5	87 ± 5	89 ± 5	63 ± 5	78 ± 5
denaturation/FCS	65 ± 5	15 ± 8	40 ± 10	90 ± 5	65 ± 5	70 ± 5
denaturation/E	*c*	19 ± 5	64 ± 5	61 ± 5	54 ± 5	86 ± 5

[a] Binding fractions obtained by FCS are compared with results from the quantitated primer extension assay (E) (%), and all hybridization extents are in % of total probe; refer to Materials and Methods for detailed description of the two hybridization protocols. [b] Hybridization extent of HS2 was too low to be reliably measured by FCS. [c] HS1 binds to the target 5′ end and cannot be extended by reverse transcriptase.

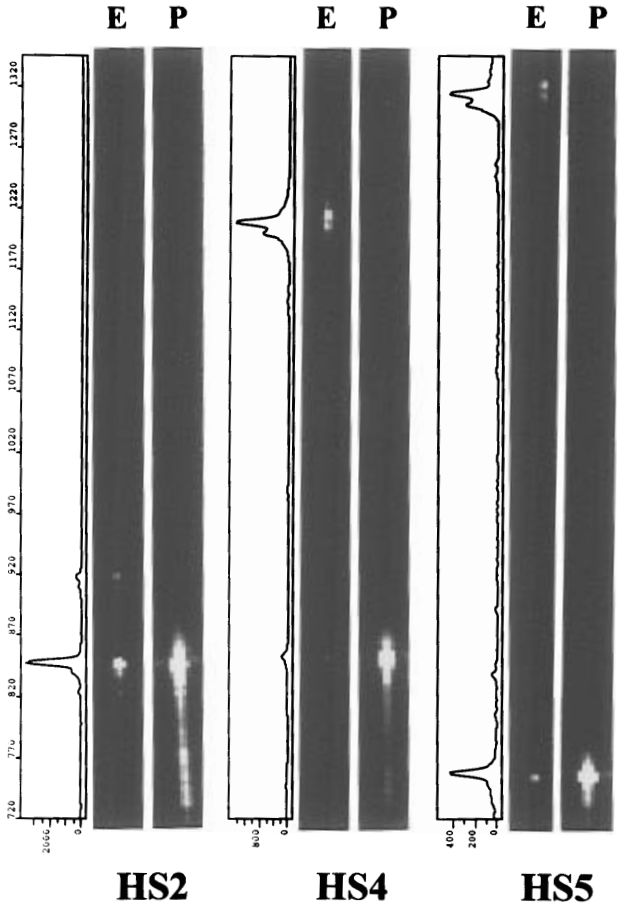

FIGURE 6: Principle of the applied quantitated primer extension assay with HS2, HS4, and HS5 as examples. After 1 h, samples from the hybridization mixtures were supplemented with dNTPs and HIV-1 reverse transcriptase, incubated over 2 min for elongation, the reactions stopped, the labeled probes precipitated and analyzed on a sequencing gel using the Genescan 672 equipment (Applied Biosystems, Weiterstadt, Germany). Lanes E were loaded with the extended probes, lanes P with the probes themselves. On the left of the lanes with extension products, the fluorescence scanning profiles are shown. HS2, HS4, and HS5 are probes showing about 10%, 90%, and 60% yield of extention product, respectively.

quantified after denaturing PAGE on an automated fluorescence sequencer. Figure 6 illustrates this novel quantitated primer extension technique. No elongation was observed without addition of target α-1 RNA, confirming the specificity of the reaction. All extension products were of the lengths expected for full extension to the target 5′ end, proving its integrity, with a characteristic double band indicating some 3′ end heterogenity, most probably due to incorporation of an additional nucleotide by the polymerase. Only between 10% and 90% of probe was elongated by HIV-1 reverse transcriptase during primer extension either after incubation with target at 40 °C for 1 h or after denaturation together with target and subsequent cooling down, with great differences between the six probes (Figure 6, Table 2). This did not essentially change with increasing duration of primer extension up to 20 min, confirming the results obtained by FCS.

Extraction of Kinetic Constants. The simplest way to interpret a limited hybridization extent as observed by FCS and primer extension assay even with target excess would be to assume a reversible hybridization reaction between probe and target with fast dissociation (Lima et al., 1992; Morrison & Stols, 1993). To have independent access to a dissociation rate constant, we tried to measure it directly by a method analogous to the label dilution method of Morrison and Stols (1993). Here, to a hybridized mixture of target and fluorescently labeled probe, a large (100 times) excess of the corresponding unlabeled probe HS1X−HS6X is added. Nevertheless, we did not find detectable dissociation for any of the probes.

By careful analysis of the hybridization kinetics of all probes, we found that they could best be described assuming a biphasic behavior with a fast initial and a slow second phase. The most simple process leading to such kinetics would imply the existence of the target RNA species RNA_f and RNA_s allowing fast and slow hybridization rates, respectively, and binding probe P with separable rate constants k_1 and k_2 to form hybrids $PRNA_f$ and $PRNA_s$, indistinguishable by FCS:

$$\mathrm{P} + \mathrm{RNA_f} \xrightarrow{k_1} \mathrm{PRNA_f}$$

$$\mathrm{P} + \mathrm{RNA_s} \xrightarrow{k_2} \mathrm{PRNA_s} \qquad (4)$$

For $k_1 \gg k_2$, this leads to the integrated rate equation

$$\frac{[\mathrm{PRNA}]_{tot}}{[\mathrm{P}]_0} = \frac{[\mathrm{PRNA_f}]}{[\mathrm{P}]_0} + \frac{[\mathrm{PRNA_s}]}{[\mathrm{P}]_0} = 1 - \frac{(1-m)}{1-m\mathrm{e}^{k_1 P_0 (m-1)t}} + \frac{(1-m)(1-\mathrm{e}^{k_2 P_0 (1-\nu)t})}{1-\frac{(1-m)}{(\nu-m)}\mathrm{e}^{k_2 P_0 (1-\nu)t}} \qquad (5)$$

with $[PRNA]_{tot}$ as the total concentration of hybrids $PRNA_f$ and $PRNA_s$, $[P]_0 \equiv P_0$, the initial probe concentration, m the ratio of initial RNA_f to initial probe concentration, $[RNA_f]_0/P_0$, and ν the ratio of total initial target to probe concentration, $[RNA]_0/P_0$, respectively. m gives a measure for the relative distribution of the two reaction paths. Fitting the observed kinetical hybridization curves with eq 5 yielded the solid curves of Figure 5. The three free fit parameters k_1, k_2, and m for the individual probes are listed in Table 3.

Direct Diffusional Analysis of Target α-1 RNA by FCS. In spite of thorough annealing of purified target α-1 RNA prior to analysis, non-denaturing PAGE as well as PACE indicated that several conformations of the RNA with different electrophoretic mobilities co-existed (data not

Table 3: Kinetic Constants k_1 and k_2 (M^{-1} s^{-1}) and Their Relative Distribution Parameter m for Hybridization of Probes HS1 and HS3−HS6 with α-1 RNA Target[a]

probe	HS1	HS3	HS4	HS5	HS6
k_1	$(1.3 \pm 0.4) \times 10^6$	$(3 \pm 1) \times 10^4$	$(3 \pm 1) \times 10^5$	$(3 \pm 0.7) \times 10^5$	$(1.5 \pm 0.5) \times 10^6$
k_2	4×10^3	*b*	4×10^3	3×10^3	1×10^3
m	0.29	0.71	0.82	0.45	0.61

[a] Probe HS2 showed a too low hybridization extent to be kinetically analyzed. $m = [RNA_f]/P_0$ and represents a measure for the distribution of the initial probe concentration P_0 on the reaction pathways with the two hypothetical RNA species RNA_f and RNA_s. [b] Probe HS3 showed a k_2 too low to be reliably measured.

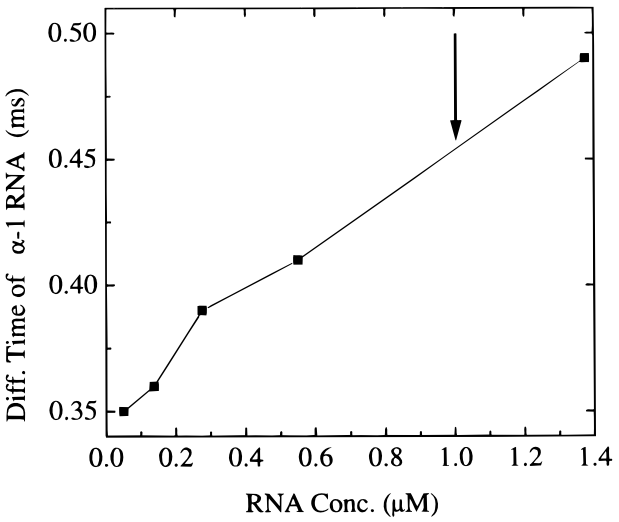

FIGURE 7: Diffusion time of target α-1 RNA in dependence of its concentration during initial denaturation in water. After cooling down, the RNA was diluted to a constant concentration in hybridization buffer including carrier DNA, and diffusion times were determined by FCS and analysis of the obtained autocorrelation curves. The standard initial RNA concentration prior to hybridization experiments was an intermediate value of 1 μM (arrow).

shown). This phenomenon has also been observed for other biologically important RNAs like group I introns at low (10 mM) $MgCl_2$ concentrations (Jaeger et al., 1991). In order to specify, whether oligomerization of α-1 RNA plays a role in forming these conformational inhomogenities, the RNA was heated in water at different concentrations, cooled down, and diluted into hybridization buffer, and the diffusion times in dependence of initial RNA concentration during denaturation were determined by FCS. Figure 7 shows that diffusion times nearly linearly increase over the examined α-1 RNA concentration range. Taking into account that diffusion times are roughly proportional to the third root of molecular weight of the diffusing species, the increase from 0.35 ms at 40 nM to 0.49 ms at 1.38 μM RNA would suggest the average formation of α-1 RNA monomers at 40 nM versus dimers or even higher oligomers by intermolecular hydrogen bonds at 1.38 μM, respectively. According to that, the presence of oligomers during the hybridization experiments must be taken into account. Since in free fitting, there was good consistency between observed complex diffusion times in calibration and hybridization measurements, the influence of probe binding to higher oligomers of RNA in the first reaction phase is shown to be of lower importance. However, it may be an explanation for the biphasic behavior, considering, e.g. RNA monomers as RNA_f and oligomers as RNA_s in eq 4.

Hybridization and Melting of TMR-Labeled DNA Double-Strands. Hybridization of TMR-labeled probes HS1−HS6 to an excess of their corresponding unlabeled cDNAs was performed as a control reaction. Table 4 indicates that for all six probes, a slight but significant increase in diffusion time upon hybridization could be observed. However, this increase was not high enough to clearly separate diffusion times of free probe and hybrid for quantitative FCS analysis of hybridization kinetics as described above for target α-1 RNA, thereby marking the limit for this kind of examination.

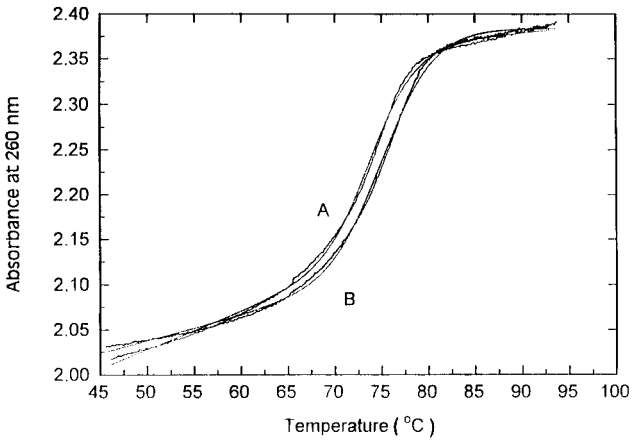

FIGURE 8: Melting curves of the labeled HS6-GSHS6 hybrid (A) in comparison with the unlabeled double-strand HS6X-GSHS6 (B, full lines). Both double-strands were measured at 5 μM in the same buffer as used in the hybridization protocols (60 mM Tris-HCl, pH 8.2, 10 mM $MgCl_2$, 10 mM KCl, 2.5 mM DTT, 2 mM spermidine). Also plotted are the best least-squares fits for the two experimental curves (smooth dotted lines). With the attached TMR label, the equilibrium melting point decreases from 73.5 (curve B) to 72.6 °C (curve A).

Table 4: Diffusion Times of Probes HS1−HS6, Free and Bound to Their Length-Matched cDNA GSHS1−GSHS6, through the Laser-Illuminated Open Volume Element of the FCS Setup in Hybridization Buffer at 40 °C (ms)

probe	HS1	HS2	HS3	HS4	HS5	HS6
free probe	0.15	0.18	0.21	0.20	0.11	0.15
bound probe	0.24	0.20	0.24	0.21	0.20	0.21

To study a possible influence of the TMR-label on hybridization of nucleic acids, the melting curve of TMR-labeled probe HS6 with its complementary unlabeled strand GSHS6 at equimolar concentrations in standard hybridization buffer was compared to that of the unlabeled HS6X/GSHS6 hybrid. Figure 8 illustrates that only a slight decrease of 0.9 °C in the presence of covalently attached TMR was found between melting points of the labeled and unlabeled double-strands.

DISCUSSION

In the present study, we used FCS-analyzed diffusion times to investigate binding kinetics of fluorescently labeled DNA probes to an artificial target RNA comprising part of the

HIV-1 genome as a model system for antisense oligonucleotide hybridization in solution. FCS proved to be a valuable tool for these kinds of studies because of (i) its high sensitivity down to the nanomolar concentration range, below which the kinetics become too slow for convenient analysis, (ii) the freedom to choose whatever buffer is desirable as long as it does not contain fluorescent contaminants, (iii) the possibility to follow hybridization in real time without separation steps for probe and hybrid, and (iv) the possibility to extract rate constants to quantitatively compare antisense oligonucleotides of interest, provided that their target is at least three to five times longer to significantly increase probe diffusion times upon hybridization.

We found, that the six probes HS1−HS6, being designed to have similar melting points with their target sequences, exhibit quite different initial association rate constants to α-1 RNA with k_1(HS6) > k_1(HS1) > k_1(HS5) ≈ k_1(HS4) > k_1(HS3) > k_1(HS2) (Figure 5; Table 3). These differences can plausibly be explained by different secondary structures of target sites and probes, thus confirming the predicted α-1 RNA structure (Figure 1). The fastest hybridizing probe is HS6, the one binding to the four non-base-paired nucleotides at the target 3′ end and to three internal loops. HS1 exhibits the second fastest association kinetics and hybridizes to six non-base-paired nucleotides at the target 5′ end and to one internal loop. HS5 is the third fastest probe. It binds to a stem−loop structure with one internal loop that represents the primer binding site of HIV-1 (though in the HIV-1 genome, the internal loop is part of a larger four-way junction). Obviously, this region is quite accessible for hybridization with an antisense sequence, a feature being essential for replication of HIV-1 (Isel et al., 1995). HS4 binds with the same rate constant as HS5, but to a higher extent. It is a long oligodeoxynucleotide hybridizing with its 3′ end to the largest internal loop of α-1 RNA and to three additional non-base-paired regions of the target. HS3 also is a long oligodeoxynucleotide and binds to the largest internal loop of the target, but both 3′ and 5′ ends of the probe bind to stems of α-1 RNA. Consequently, HS3 exhibits the second lowest rate constant. All five probes, HS1 and HS3−HS6, only show few base pairs in their own secondary structure prediction with largely single-stranded 3′ ends (Figure 1). Unlike these probes, HS2 as the least efficient binder has a tight stem−loop structure. This structure can interact with α-1 RNA only via a six-bases loop that is complementary to a similar structure in the target, while the rest of the target is hidden in a stem. These observations correspond very well with earlier studies on the pairing pathway of antisense nucleic acids, in which the binding process starts with a loop−loop interaction (called the "kissing complex"), and complete hybridization requires an additional interaction that involves single-stranded regions of both target and antisense nucleic acid (Siemering et al., 1994; Hjalt & Wagner, 1995). Consequently, the more internal loops and single-stranded regions are involved, the faster a hybridization will be (Lima et al., 1992), though tertiary interactions also play a role (Kumazawa et al., 1992; Zarrinkar & Williamson, 1994). Association rate constants of 10^6 M^{-1} s^{-1} as obtained for HS6 and HS1 in our study are thus among the highest known for antisense/RNA pairs.

As used in our study, FCS can only quantify overall hybridization kinetics by monitoring the distribution between free and stably bound probe. To account for the obtained complex kinetics with a fast initial and a slow second phase, for which we had evidence from both FCS and primer extension assays (Table 2), we had to assume a biphasic irreversible reaction. This is in contrast to an earlier study using FCS on an 18mer DNA probe hybridizing to a 7.5 kb long DNA target (Kinjo & Rigler, 1995), where monophasic irreversible kinetics were assumed, rapidly leading to 100% binding. Several reasons might account for this difference: (i) hybridization to a 400 times longer target results in a hybrid with a 20 times longer diffusion time, with little relative deviations masking small fractions of unbound probe; (ii) in the DNA−DNA hybridization study a single probe against a sequencing primer site was used, that can be expected to exhibit extraordinary fast and complete binding; (iii) hybridization of DNA to DNA is less complex than that of DNA to RNA due to fewer secondary and tertiary interactions within a DNA target. Our findings also contrast with other studies, where reversible hybridization kinetics have been proposed (Lima et al., 1992; Morrison & Stols, 1993). While we worked with rather long (17mer to 37mer) probes suitable as specific antisense agents and could not detect a significant dissociation from their target, in these earlier studies reversible hybridization was found for short (10mer) probes binding to short, low-structured DNA or RNA targets. Indeed, earlier studies on hybridization of long mRNAs with their cDNAs led to a complex multiphasic behavior similar to our results that was interpreted as a consequence of different sequence complexities of target sites (Young & Anderson, 1985).

A further hint for hybridization in our model system to be more complex than represented either by a single irreversible or reversible reaction of two species, is the fact that the relative contribution of the two reaction paths characterized by the ratio $m = [RNA_f]/P_0$ significantly differ between probes (Table 3). In this context it is necessary to keep in mind that both probe and target themselves are flexible structures that can co-exist in different secondary and tertiary structure conformations as found for other RNAs (Jaeger et al., 1991). In our system, evidence can be found from direct diffusional analysis of target α-1 RNA revealing different diffusing species in dependence of initial RNA concentration, an observation indicating multimolecular rather than unimolecular processes (Figure 7). Some of these conformations could lead to less accessible target sequences (Parkhurst & Parkhurst, 1995), resulting in separable phases in the overall reaction kinetics as the conformations react with different velocities. For probes with different target sites the contributions of different conformational species to the initial and second reaction phase can be expected to differ as experimentally observed. Thus, identification of different phases in hybridization as due to at least two different RNA conformations present in α-1 RNA preparations is a quite attractive interpretation of our results, though more complex reaction pathways resulting in biphasic behavior cannot be excluded. More detailed examination of the kinetics over a long time range could help to further elucidate the underlying reaction mechanisms. This will be a subject of further investigations. Since other kinetic interpretation models of limited hybridization extent, like the assumption of a totally unreactive RNA fraction, gave similar values for the initial association constants, the model applied here proved to be of lower importance for comparison of different probes with one another.

Antisense nucleic acids normally are not fluorescently labeled as the probes necessary for FCS analysis (Figure 2). We only found a subtle decrease of equilibrium melting points of our probes with length-matched cDNA upon coupling to the TMR label (Figure 8). Moreover, there is evidence that tetramethylrhodamine interacts with the nucleobases of an attached oligonucleotide (Bob Clegg, MPI, Göttingen, personal communication), so that an influence of the label on values of hybridization kinetic constants cannot be excluded. The relative comparison of kinetics of a set of antisense nucleic acids against a common target, however, should be unaffected by such an influence.

We therefore conclude that FCS is an appropriate tool for rapid screening for suitable antisense nucleic acids effective against targets of interest like HIV-1 RNA. After rapidly hybridizing probes were found, these could also be used to rapidly trace the presence of a sequence element by FCS, e.g., for detection of RNA by solution hybridization (Coutlee et al., 1990) or the automated analysis of mixed microbial populations in suspensions (Wallner et al., 1993). Moreover, by comparison of hybridization efficiencies of probes against different target regions, indirect evidence for predicted secondary structure elements might be possible. Using two probes simultaneously, one could identify higher-order structures by analyzing whether the binding of a fluorescently labeled probe is facilitated by preceding hybridization of an unlabeled probe to a distant target site. Easy synthetic or enzymatic access to suitable non-radioactive probes, low consumption of probe and target, free eligibility of additional probe modifications and hybridization buffer (even cellular extracts could be used) are important advantages of the method. We believe that this will extend the envisaged scope of fluorescence correlation spectroscopy applications (Eigen & Rigler, 1994; Rigler, 1995).

ACKNOWLEDGMENT

We thank Dr. Magda Pop for donation of α-1 RNA, Sylvia Völker and Dr. Günther Strunk for analysis of fluorescently labeled probes by HPLC, Dr. Dietmar Pörschke for measuring DNA melting curves, Dr. Said Modaressi for assistance with the GENESCAN Software, Prof. Rudolf Rigler for help in constructing the FCS setup, Prof. Fritz Eckstein and Dr. Franz-Josef Meyer-Almes for critical reading of the manuscript, and Prof. Manfred Eigen for a very stimulating environment.

APPENDIX

Deduction of the Fitting Function

Given the competitive reactions

$$\mathrm{RNA_f} + \mathrm{P} \xrightarrow{k_1} \mathrm{PRNA_f}$$

$$\mathrm{RNA_s} + \mathrm{P} \xrightarrow{k_2} \mathrm{PRNA_s}$$

with initial conditions for each component

fast: $[\mathrm{RNF_f}]_0 \equiv \mathrm{RNA_f}|_0 = m[\mathrm{P}]_0 \equiv mP_0$

slow: $[\mathrm{RNF_s}]_0 \equiv \mathrm{RNA_s}|_0 = nP_0$

total: $[\mathrm{RNA}]_{\mathrm{tot}} = (m+n)P_0 = \nu P_0$

The relation for irreversible reactions is given by

$$[\mathrm{PRNA_s}] = \mathrm{RNA_s}|_0 - \mathrm{RNA_s}|_0\left(1 - \frac{[\mathrm{PRNA_f}]}{\mathrm{RNA_f}|_0}\right)^{k_2/k_1} \quad \text{(A1)}$$

For $k_2 \ll k_1$ it follows that for the reaction of the fast component, $[\mathrm{PRNA_s}] = 0$. This allows for small k_2/k_1 a separation in two time ranges.

first time range

$$\frac{\mathrm{d}[\mathrm{PRNA_f}]}{\mathrm{d}t} = k_1[\mathrm{P}](\mathrm{RNA_f}|_0 - [\mathrm{PRNA_f}])$$

$$\Rightarrow \frac{\mathrm{d}[\mathrm{PRNA_f}]}{\mathrm{d}t} = k_1(P_0 - [\mathrm{PRNA_f}])(\mathrm{RNA_f}|_0 - [\mathrm{PRNA_f}])$$

With $\mathrm{RNA_f}|_0 = mP_0$ and $[\mathrm{PRNA_f}] \equiv Y$

$$\frac{\mathrm{d}Y}{Y^2 - Y(m+1)P_0 + m{P_0}^2} = k_1\mathrm{d}t$$

With $X = ax^2 + bx + c$,

$$\int\frac{\mathrm{d}x}{X} = \frac{1}{\sqrt{b^2-4ac}}\ln\frac{2ax+b-\sqrt{b^2-4ac}}{2ax+b+\sqrt{b^2-4ac}}$$

it follows that

$$\frac{1}{(m-1)P_0}\ln\frac{Y-P_0m}{Y-P_0} = k_1t + C$$

under the condition that

$$Y(0) = 0 \Rightarrow C = \frac{1}{(m-1)P_0}\ln m$$

$$\Rightarrow \frac{[\mathrm{PRNA_f}]}{P_0}(t) = 1 - \frac{(1-m)}{1-m\mathrm{e}^{k_1P_0(m-1)t}} \quad \text{(A2)}$$

second time range (the initial amount of probe is reduced by fraction of m)

$$\frac{\mathrm{d}[\mathrm{PRNA_s}]}{\mathrm{d}t} = k_1(P_0(1-m) - [\mathrm{PRNA_s}])(\mathrm{RNA_s}|_0 - [\mathrm{PRNA_s}])$$

with $\mathrm{RNA_s}|_0 = (\nu - m)P_0$ and $[\mathrm{PRNAs}] \equiv Y$

$$\Rightarrow \frac{\mathrm{d}Y}{Y^2 - Y(1-2m+\nu)P_0 + (1-m)(\nu-m){P_0}^2} = k_2\mathrm{d}t$$

$$\Rightarrow \frac{1}{P_0(1-\nu)}\ln\frac{Y-P_0(1-m)}{Y-P_0(\nu-m)} = k_2t + C$$

$$Y(0) = 0 \Rightarrow C = \frac{1}{P_0(1-\nu)}\ln\frac{(1-m)}{(\nu-m)}$$

$$\Rightarrow \frac{[\mathrm{PRNA_s}]}{P_0} = \frac{(1-m)(1-\mathrm{e}^{k_2P_0(1-\nu)t})}{1-\frac{(1-m)}{(\nu-m)}\mathrm{e}^{k_2P_0(1-\nu)t}} \quad \text{(A3)}$$

The total reaction is given by the sum of eqs A2 and A3:

$$\frac{[\mathrm{PRNA}]_{\mathrm{tot}}}{P_0} = \frac{[\mathrm{PRNA_f}]}{P_0} + \frac{[\mathrm{PRNA_s}]}{P_0} = 1 - \frac{(1-m)}{1-m\mathrm{e}^{k_1 P_0 (m-1)t}} + \frac{(1-m)(1-\mathrm{e}^{k_2 P_0 (1-\nu)t})}{1 - \frac{(1-m)}{(\nu-m)}\mathrm{e}^{k_2 P_0 (1-\nu)t}}$$

REFERENCES

Bishop, J. O., Morton, J. G., Rosbash, M., & Richardson, M. (1974) *Nature 250*, 199−202.

Breslauer, K. J. (1986) in *Thermodynamic Data for Biochemistry and Biotechnology* (Hinz, H.-J., Ed.) pp 402−427, Springer-Verlag, New York.

Briggs, J., Elings, V. B., & Nicoli, D. F. (1981) *Science 212*, 1266−1267.

Britten, R. J., & Kohne, D. E. (1968) *Science 161*, 529−540.

Bush, C. A. (1974) in *Basic Principles in Nucleic Acid Chemistry* (Ts'o, P. O. P., Ed.) Vol. 2, pp 91−169, Academic Press, New York.

Coutlee, F., Rubalcaba, E. A., Viscidi, R. P., Gern, J. E., Murphy, P. A., & Lederman, H. M. (1990) *J. Biol. Chem. 265*, 11601−11604.

Crooke, S. T. (1992) *Annu. Rev. Pharmacol. Toxicol.* 32, 329−376.

Dewanjee, M. K., Ghafouripour, K., Kapadvanjwala, M., & Samy, A. T. (1994*) BioTechniques 16*, 844−850.

Dropulic, B., & Jeang, K. T. (1994) *Hum. Gene Ther. 5*, 927−939.

Ehrenberg, M., & Rigler, R. (1974) *J. Chem. Phys. 4*, 390−401.

Eigen, M., & Rigler, R. (1994) *Proc. Natl. Acad. Sci. U.S.A. 91*, 5740−5747.

Elson, M. E., & Magde, D. (1974) *Biopolymers 13*, 1−27.

Gebinoga, M., & Oehlenschläger, F. (1996) *Eur. J. Biochem. 235*, 256−261.

Hjalt, T. A. H., & Wagner, E. G. H. (1995) *Nucleic Acids Res. 23*, 580−587.

Hofacker, I. L., Fontana, W., Stadler, P. F., Bonhoeffer, L. S., Tacker, L., & Schuster, P. (1994) *Monatsh. Chem. 125*, 167−188.

Inouye, M. (1988) *Gene 72*, 25−34.

Isel, C., Ehresmann, C., Keith, G., Ehresmann, B., & Marquet, R. (1995) *J. Mol. Biol. 247*, 236−250.

Jaeger, L., Westhof, E., & Michel, F. (1991) *J. Mol. Biol. 221*, 1153−1164.

Kati, W. M., Johnson, K. A., Jerva, L. F., & Anderson, K. S. (1992) *J. Biol. Chem. 267*, 25988−25997.

Kinjo, M., & Rigler, R. (1995) *Nucleic Acids Res. 23*, 1795−1799.

Koppel, D. (1974) *Phys. Rev. A 10*, 1938−1945.

Kumazawa, Y., Yokogawa, T., Tsurui, H., Miura, K., & Watanabe, K. (1992). *Nucleic Acids Res. 20*, 2223−2232.

Li, Y., Bevilacqua, P. C., Mathews, D., & Turner, D. H. (1995) *Biochemistry 34*, 14394−14399.

Lima, W. F., Monia, B. P., Ecker, D. J., & Freier, S. M. (1992) *Biochemistry 31*, 12055−12061.

Ma, C. K., Kolesnikow, T., Rayner, J. C., Simons, E. L., Yim, H., & Simons, R. W. (1994) *Mol. Microbiol. 14*, 1033−1047.

Magde, D., Elson, E. L., & Webb, W. W. (1972) *Phys. Rev. Lett. 29*, 705−708.

Magde, D., Elson, E. L., & Webb, W. W. (1974) *Biopolymers 13*, 29−61.

Manoharan, M., Tivel, K. L., Zhao, M., Nafisi, K., & Netzel, T. L. (1995) *J. Phys. Chem. 99*, 17461−17472.

Milligan, J. F., Groebe, D. R., Witherell, G. W., & Uhlenbeck, O. C. (1987) *Nucleic Acids Res. 15*, 8783−8798.

Mills, D. R., Kramer, F. R., Dobkin, C., Nishihara, T., & Cole, P. E. (1980) *Biochemistry 19*, 228−236.

Morrison, L. E., & Stols, L. M. (1993) *Biochemistry 32*, 3095−3104.

Müller, B., Restle, T., Weiss, S., Gautel, M., Sczakiel, G., & Goody, R. (1989) *J. Biol. Chem. 264*, 13975−13978.

Palmer, A. G., & Thompson, N. L. (1989) *Chem. Phys. Lipids 50*, 253−270.

Parkhurst, K. M., & Parkhurst, L. J. (1995) *Biochemistry 34*, 285−292.

Patel, D. J., Pardi, A., & Itakura, K. (1982) *Science 216*, 581−590.

Pop, M. P. (1995) *Impact of Sequence on HIV-1 Reverse Transcription*, Cuvillier Verlag, Göttingen, Germany.

Pörschke, D., & Jung, M. (1982) *Nucleic Acids Res. 10*, 6163−6176.

Qian, H., & Elson, E. L. (1991) *Appl. Opt. 30*, 1185−1195.

Rigler, R. (1995) *J. Biotechnol. 41*, 177−186.

Rigler, R., Widengren, J., & Mets, Ü. (1992) in *Fluorescence Spectroscopy* (Wolfbeis, O. S., Ed.) pp 13−21, Springer Verlag, Berlin.

Rigler, R., Mets, Ü., Widengren, J., & Kask, P. (1993) *Eur. Biophys. J. 22*, 169−175.

Siemering, K. R., Praszkier, J., & Pittard, A. J. (1994) *J. Bacteriol. 176*, 2677−2688.

Simons, R. W. (1988) *Gene 72*, 35−44.

Thompson, N. L. (1991) in *Topics in Fluorescence Spectroscopy* (Lakowicz, J. R., Ed.) Vol. 1, pp 337−378, Plenum Press, New York.

van der Krol, A. R., Mol, J. N. M., & Stuitje, A. R. (1988) *Gene 72*, 45−50.

Varani, G. (1995) *Annu. Rev. Biophys. Biomol. Struct. 24*, 379−404.

Wagner, E. G. H., & Simons, R. W. (1994) *Annu. Rev. Microbiol. 48*, 713−742.

Wagner, R. W. (1994) *Nature 372*, 333−335.

Wallner, G., Aman, R., & Beisker, W. (1993) *Cytometry 14*, 136−143.

Walter, N. G., & Strunk, G. (1994) *Proc. Natl. Acad. Sci. U.S.A. 91*, 7937−7941.

Widengren, J., Rigler, R., & Mets, Ü. (1994). *J. Fluorescence 4*, 255−258.

Widengren, J., Mets, Ü., & Rigler, R. (1995) *J. Phys. Chem. 99*, 13368−13379.

Yang, M. T., Scott, H. B., & Gardner, J. F. (1995) *J. Biol. Chem. 270*, 23330−23336.

Young, B. D., & Anderson, M. L. M. (1985) in *Nucleic Acid Hybridisation*: *A Practical Approach* (Hames, B. D., & Higgins, S. J., Eds.) pp 47−71, IRL Press, Oxford.

Zarrinkar, P. P., & Williamson, J. R. (1994) *Science 265*, 918−924.

BI960517G